Applied Catalysis B: Environmental 331 (2023) 122733

Contents lists available at ScienceDirect

Applied Catalysis B: Environmental

journal homepage: www.elsevier.com/locate/apcatb

A high-cyano groups-content amorphous-crystalline carbon nitride isotype heterojunction photocatalyst for high-quantum-yield H_2 production and enhanced CO_2 reduction

Cheng Cheng [a,b], Liuhao Mao [a], Xing Kang [a], Chung-Li Dong [c], Yu-Cheng Huang [c], Shaohua Shen [a], Jinwen Shi [a,d,*], Liejin Guo [a]

[a] State Key Laboratory of Multiphase Flow in Power Engineering (MFPE), International Research Center for Renewable Energy (IRCRE), Xi'an Jiaotong University (XJTU), 28 West Xianning Road, Xi'an 710049, China
[b] School of Chemical Engineering and Technology, Xi'an Jiaotong University (XJTU), 28 West Xianning Road, Xi'an 710049, China
[c] Department of Physics, Tamkang University, 151 Yingzhuan Road, Tamsui 25137, Taiwan, China
[d] Integrated Energy Institute, Sichuan Digital Economy Industry Development Research Institute, 88 Jiefang Road, Chengdu 610036, China

ARTICLE INFO

Keywords:
Carbon dioxide
Crystallinity
Hydrogen
Eutectic salt
Solar energy

ABSTRACT

Polymeric carbon nitride suffers terrible recombination of photo-generated carriers and thus usually results in limited photocatalytic activity. Improving crystallinity and creating novel structure can effectively alleviate the aforementioned problem. Herein, a high-cyano groups-content and amorphous-crystalline carbon nitride isotype heterojunction (BCN-NaK) was obtain via a post treatment strategy in eutectic salt. The cyano groups acted as electron acceptors, and the intimate isotype heterojunction constructed by amorphous carbon nitride and crystalline poly-heptazine-imide built interfacial electric field. Both synergistically enabled BCN-NaK more efficient charge transfer than other amorphous and crystalline carbon nitrides. Comprehensive and systematic analysis demonstrated that the promoted charge transfer made the predominant contribution to the ultrahigh photocatalytic H_2-production activity of BCN-NaK with an excellent apparent quantum yield of 68.9 % at 405 nm. In addition, BCN-NaK exhibited a good photocatalytic CO_2-to-CO conversion rate of 22.8 μmol h^{-1} g_{cat}^{-1} without adding sacrificial agent or loading metal under visible light.

1. Introduction

The indiscriminate and massive consumption of fossil fuels has induced severe global energy crisis and environmental issues [1,2]. A promising way to address the problem is to develop clean and sustainable energy which also can reduce CO_2 emission. Converting solar energy into H_2 via photocatalysis from water splitting is an ideal technology of sustainable energy conversion [3,4]. Primarily, the pivotal challenge for this technology is designing robust, efficient and cost-effective photocatalyst. Among different kinds of developed photocatalysts, polymeric carbon nitride (PCN) shows as a promising candidate for the practical application of photocatalytic H_2 production due to its significant advantages of low cost, favorable stability and visible-light response [5–7].

As a prototypical polymer, PCN is normally obtained by traditional thermal-induced polymerization method and typically possesses amorphous, the local structure is disordered, and the exciton binding energy is large [8,9]. Consequently, PCN suffers terrible recombination of photo-generated carriers, which is the dominant obstruction that need to be eliminated urgently for improving the photocatalytic performance [10–12]. To address the shortcomings of PCN for obtaining high photocatalytic efficiency, a myriad of strategies have been explored over the past decade, such as crystallinity regulation [9,13–15], copolymerization [16–18], nanostructure engineering [19,20], doping [21,22] and heterojunction design [23,24]. However, the currently reported photocatalytic efficiency is still far from practical application, more feasible modifications and structure regulations of PCN are continued efforts to make new breakthrough for activity. Recently, a molten salt-based strategy has been developed to obtain high crystalline carbon nitride, improving the crystallinity of carbon nitride can effectively reduce the

* Corresponding author at: State Key Laboratory of Multiphase Flow in Power Engineering (MFPE), International Research Center for Renewable Energy (IRCRE), Xi'an Jiaotong University (XJTU), 28 West Xianning Road, Xi'an 710049, China.
E-mail address: jinwen_shi@mail.xjtu.edu.cn (J. Shi).

https://doi.org/10.1016/j.apcatb.2023.122733
Received 1 January 2023; Received in revised form 20 March 2023; Accepted 2 April 2023
Available online 4 April 2023

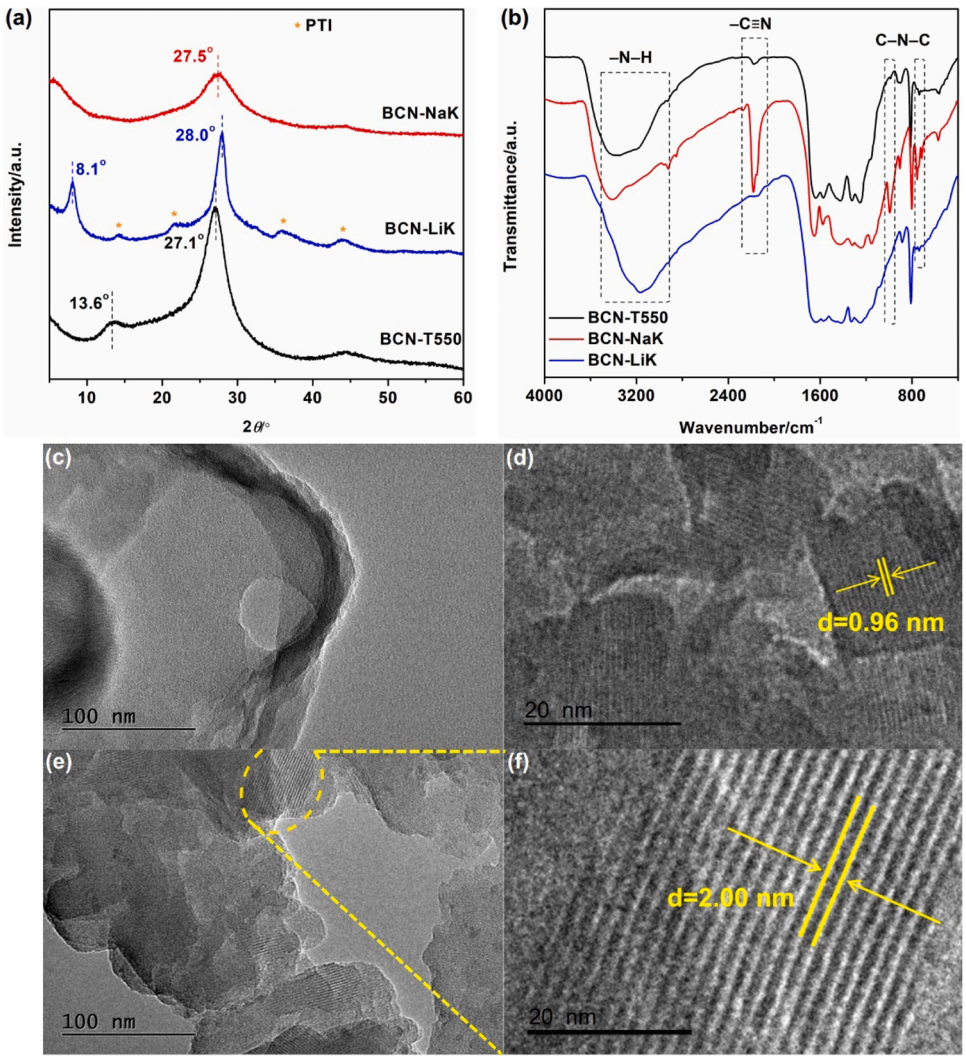

Fig. 1. (a) XRD patterns and (b) FTIR spectra of BCN-T550, BCN-LiK and BCN-NaK. (c-f) TEM images of (c) BCN-T550, (d) BCN-LiK and (e, f) BCN-NaK. (f) was the magnified result for the circled area in (e). Scale bar: (c, e) 100 nm, (d, f) 20 nm.

recombination centers and accelerate the transfer of the photo-generated carriers [25–27]. Moreover, high crystallinity also can extend π-conjugated system and increase delocalized π-electrons, resulting in increased charge migration rate. Wang et al. took urea as precursor and NaCl/KCl as eutectic salt to prepare high crystalline carbon nitride, and the apparent quantum yield (AQY) for photocatalytic H_2 production can reach 60 % at 420 nm [9]. In addition, constructing cyano groups in carbon nitride structure is also an effective way for facilitating charge transfer because cyano groups can act as electron acceptors [28,29]. Ye at al. reported that introducing cyano groups into carbon nitride structure achieved highly efficient charge transfer and resulted in significantly enhanced photocatalytic H_2 production activity [30].

Meanwhile, constructing heterojunctions of two semiconductors with appropriate energy band alignment to build an interfacial electric field is generally an effective approach to promoting charge carriers separation [7]. Particularly, isotype heterojunction can realize intimate interface contact and low interface resistance, its strong interfacial electric field results in effective charge separation [30–32]. Eutectic-salt post treatment is an efficient in-situ approach to prepare carbon nitride isotype heterojunction because the adjustable salt compositions and melting points [33]. Meanwhile, eutectic salt post treatment is a common method to obtain high crystalline carbon nitride. Crystalline poly-triazine-imide (PTI) could be prepared under the molten salt of LiCl/KCl which has low melting point (MP = 352 °C) [9,33], while stable and active crystalline poly-heptazine-imide (PHI) could be obtained under the eutectic salt of NaCl/KCl which has high melting point (MP = 652 °C) [14]. Exploring proper way to construct carbon nitride isotype heterojunction with integration of high crystallinity and high cyano groups content could alternatively achieve outstanding photocatalytic efficiency.

Previously, we have developed a cyano groups modified disordered carbon nitride (BCN) whose AQY for photocatalytic H_2 production achieved a high value of 45.5 % at 420 nm [34]. Based on the previous work, furtherly improving the charge carriers utilization is hope to make breakthrough in photocatalytic efficiency. Motivated by the above thoughts, herein, eutectic salt post treatment was put forward to convert BCN into an amorphous-crystalline isotype heterojunction with increased content of cyano groups. The *in-suit* way resulted in intimately chemical bonding for heptazine-based amorphous carbon nitride and crystalline PHI, and energy band alignments induced strong interfacial electric field within the isotype heterojunction, consequently resulting in significantly enhanced photocatalytic H_2-production efficiency. Systematic analyses were carried out to investigate the structure of the isotype heterojunction and mechanism for the enhanced charge carrier utilization.

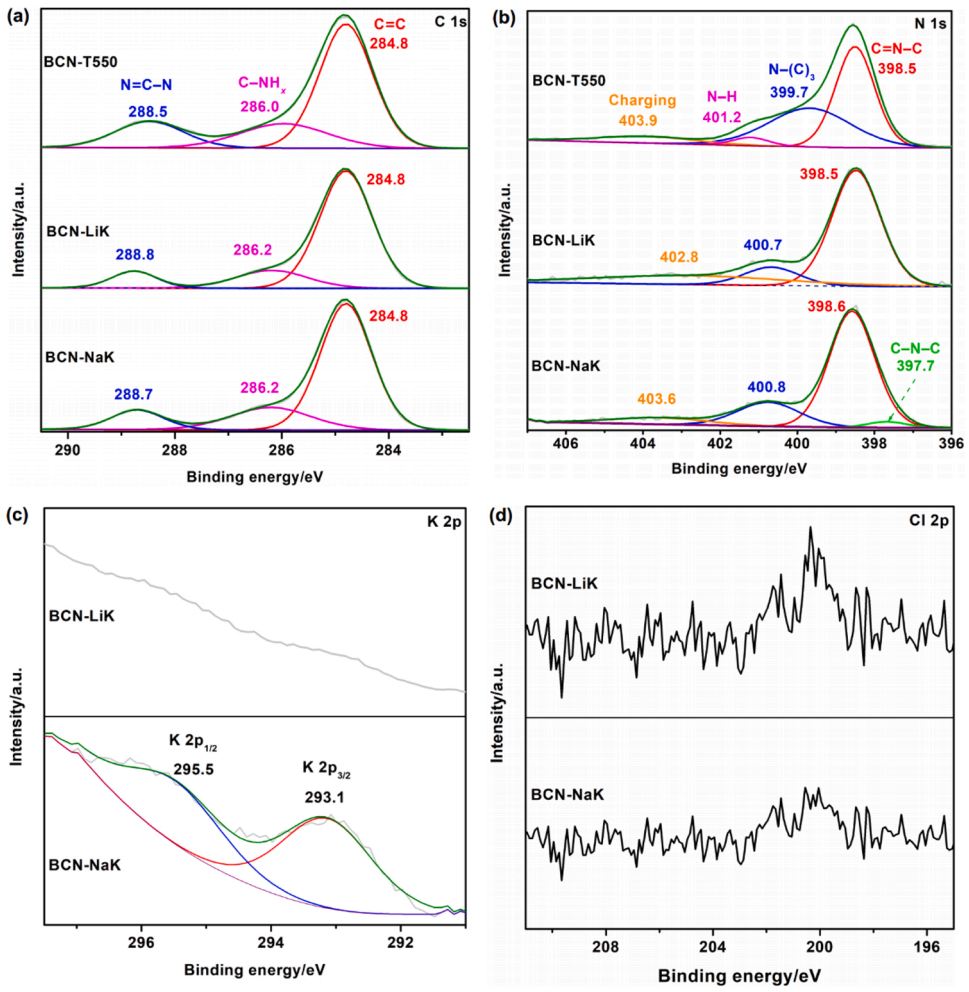

Fig. 2. (a, b) High-resolution XPS spectra of (a) C 1 s and (b) N 1 s for BCN-T550, BCN-LiK and BCN-NaK. (c, d) High-resolution XPS spectra of (c) K 2p and (d) Cl 2p for BCN-LiK and BCN-NaK.

2. Experimental section

2.1. Photocatalyst preparation

Biuret (2 g) was placed into a clean alumina crucible with cover and calcined at 500 °C (ramping rate, 5 °C min^{-1}) for 2 h under Ar atmosphere. After cooling down to room temperature, the intermediate melon product (denoted as BCN-500) was collected for further use. Subsequently, the intermediate melon product (60 mg) was mixed with NaCl (430 mg) and KCl (170 mg) and ground together to generate a homogeneous solid mixture. The mixture was then further calcined at 550 °C for another 2 h under Ar atmosphere. After natural cooling, the obtained mixture was washed with DI water to remove the metal salts and then collected after drying under vacuum at 50 °C. The final product was denoted as BCN-NaK. Other products (denoted as BCN-Li, BCN-Na and BCN-K, respectively) were prepared with the similar procedure of BCN-NaK except that NaCl/KCl was replaced by 600 mg of LiCl, NaCl and KCl, respectively. Amorphous carbon nitride (ACN) was prepared by just calcining the intermediate melon product (60 mg) at 550 °C for 2 h under Ar atmosphere, and the obtained product was denoted as BCN-T550. Crystalline carbon nitride was prepared with the similar procedure of BCN-NaK except that NaCl/KCl was replaced by LiCl/KCl (LiCl: 270 mg and KCl: 330 mg), and the obtained product was denoted as BCN-LiK.

Materials, Sample characterization, Photocatalytic performance measurement, AQY measurement, Photo(electro)chemical measurement and Computational method were supplemented in the Supplementary Material.

3. Results and discussion

3.1. Structure for photocatalysts

Eutectic salts with different melting points modulate the polymerization process of carbon nitride quite differently. LiCl/KCl eutectic salt has the melting point (352 °C) well below the typical polymerization temperature of PCN (T = 550 °C), and it can provide an inert liquid environment to enable the solid reactants sufficient condensation and favorable mass transfer [9,27]. While NaCl/KCl is not liquated during the polymerization process due to its high melting point (652 °C), it plays the role as a salt crystal template agent [9]. Therefore, NaCl/KCl is considered to promote PCN partial crystallization, and no lithium would avoid the PTI formation, otherwise crystalline PHT obtains [35].

As shown from the X-ray diffraction (XRD) patterns (Fig. 1a), without eutectic salt, BCN-T550 showed typical diffraction peaks of heptazine-based graphitic carbon nitride (g-C_3N_4) and demonstrated long-range disordered structures in atomic arrangements, which was in accordance with our previous work and indicated only post annealing of BCN-500 did not significantly change the crystal phase structure and crystallinity (Fig. S1) [34]. For the crystalline carbon nitride, BCN-LiK showed different peak positions from BCN-T550. Two obvious peaks at 8.1° and 28.0°, corresponding to in-plane repeating units of continuous heptazine framework and the inter-layer stacking of conjugated

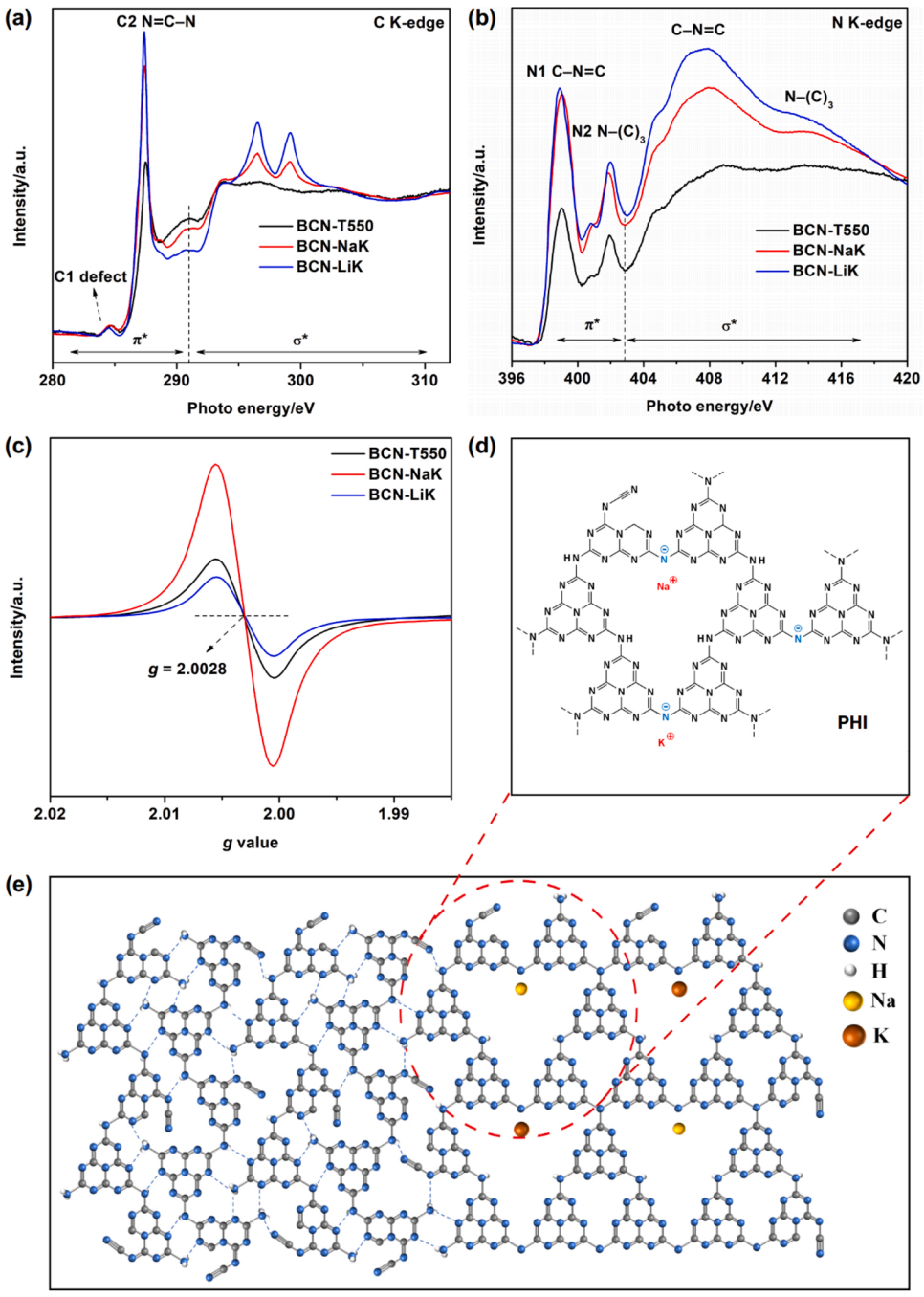

Fig. 3. (a) C and (b) N K-edge XANES spectra, and (c) EPR spectra for BCN-T550, BCN-NaK and BCN-LiK. (d, e) Proposed molecular structure of (d) PHI and (e) BCN-NaK.

aromatic systems, respectively, were observed, indicating that the dominate component of BCN-LiK was heptazine-based crystalline PHI [15,36]. Besides, due to the existence of lithium, several weak characteristic peaks attributed to the triazine-based PTI appeared in the XRD patterns of BCN-LiK (Fig. S2) [33,37]. The results demonstrated that BCN-LiK possessed the structure of crystalline heptazine-triazine isotype heterojunction. Interestingly and significantly, BCN-NaK exhibited a single (002) peak in the XRD pattern, but (100) peak was almost disappeared. The absence of (100) peak was presumably caused by NaCl/KCl, which promoted the partial structural evolution of heptazine framework under specific synthetic process and led to local disordered structure or embedded defect groups into the in-planes (Fig. S3) [14]. Fourier transform infrared spectra (FTIR) were investigated to further disclose the structure features of the carbon nitrides, as shown in Fig. 1b. Because BCN-LiK contained dominate heptazine-based structure, all the samples equally consisted of basic tri-s-triazine (heptazine)-similar frameworks [38]. Specially and importantly, a distinctly peak at 2178 cm^{-1} which was assigned to the asymmetric stretching vibration of cyano groups (–C≡N) was obviously presented in BCN-NaK spectra [30], and the peak intensity was significantly stronger than those in the others. Therefore, this results clearly indicated lots of cyano-terminal –C≡N functional groups were pervasively existed in the frameworks of BCN-NaK. In addition, the peak at 784 cm^{-1} of BCN-NaK showed stronger intensity than those of the others, and a solely new absorption peak at 1065 cm^{-1} appeared for BCN-NaK with strong intensity. The two peaks were related to symmetric and asymmetric vibration of $–NC_2$

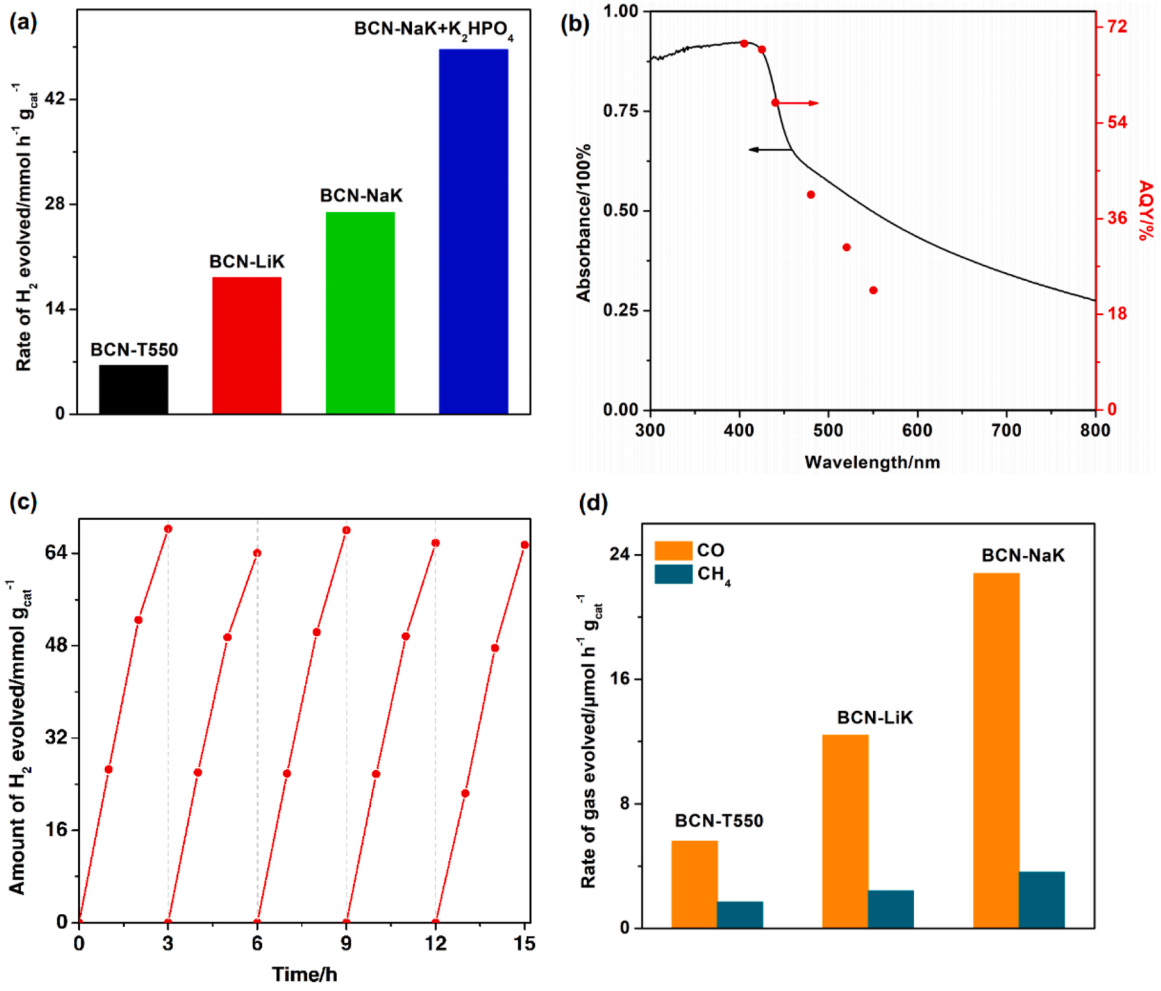

Fig. 4. (a) Photocatalytic H_2-production activities for BCN-T550, BCN-LiK, BCN-NaK and BCN-NaK+K_2HPO_4 under visible-light irradiation ($\lambda > 400$ nm). (b) Wavelength-dependence AQYs for BCN-NaK+K_2HPO_4. (c) Photocatalytic H_2- production stability test of BCN-NaK under visible-light irradiation ($\lambda > 400$ nm). (d) Photocatalytic CO_2 reduction activities for BCN-T550, BCN-LiK and BCN-NaK. "BCN-NaK+K_2HPO_4" represented the photocatalytic H_2-production test for BCN-NaK by adding 0.08 mol of K_2HPO_4 in the reaction solution while keeping other measurement conditions the same.

bonds in metal–NC_2 groups, thus revealing that the cations (e.g., K^+ or Na^+) with large atomic sizes were incorporated into heptazine-based rings or integrated in interlayer of BCN-NaK structure [14].

Structural insight based on transmission electron microscopy (TEM) provides compelling evidence to specify the crystallinity of carbon nitride. It is commonly accepted that crystalline materials show well-resolved lattice features with a bunch of ordered lattice fringes whereas amorphous materials do not. According to the TEM images, Fig. 1c presents the TEM image of BCN-T550, which showed the typical amorphous structural feature and appeared as layer structure. Another BCN-LiK showed well-resolved lattice fringes (Fig. 1d), and the lattice fringe of 0.96 nm was recorded and corresponded to the (100) plane of heptazine-based crystalline carbon nitride [9]. In Fig. 1e, BCN-NaK showed a structure of amorphous-crystalline carbon nitride junction, the partially crystallized carbon nitride had the lattice fringe of 2.00 nm which attributed to PHI structure (Fig. 1f) [35,39]. Consequently, the results intuitively demonstrated BCN-NaK had high-cyano group-s-content and amorphous-crystalline isotype heterojunction.

More structure information of the carbon nitrides were investigated by X-ray photoelectron spectroscopy (XPS). As shown in Fig. 2a, all the carbon nitrides showed similar C 1 s spectra, the peaks could be fitted and indexed to standard carbon C═C, sp^2-hybridized C in C–NH_x, and sp^2 C linked to N in N – C═N, respectively [40,41]. The similar results indicated BCN-T550, BCN-LiK and BCN-NaK all had the dominate heptazine-based structures. For the N 1 s spectra (Fig. 2b), the peaks of BCN-T550 could be fitted and indexed to the sp^2-nitrogen in N – C═N ($N_{2\,C}$), tertiary nitrogen in N – $(C)_3$ ($N_{3\,C}$) groups, nitrogen in heterocycles N – H and charging effect, respectively [16,38], which all belonged to typical characteristic peaks of g-C_3N_4. While the N 1 s spectrum for BCN-LiK only showed three characteristic peaks, the peak related to amino functions (N – H), which originated from terminal amino groups of carbon nitride frameworks, was disappeared. In addition, the peak of N – $(C)_3$ for BCN-LiK located at evident higher binding energy as compared to that of BCN-T550. The results indicated eutectic salts could greatly influence the structure of carbon nitride and promote sufficient condensation of reactants. For BCN-NaK, firstly, a peak at 397.7 eV was exclusive and assigned to tertiary nitrogen in negatively charged –NC_2 groups (N–C–N) [14], which neutralized the cations. Secondly, BCN-NaK was also absence of the peak related to amino functions (N – H), it could conclude to be ascribed to the formation of cyano groups. Because $N_{2\,C}$ and $N_{3\,C}$ participate in the construction of the basic heptazine heterocyclic ring (C_6N_7) substructure for carbon nitride, the larger peak-area ratio of sp^2 C–N = C bonds to the sum of sp^3 N – $(C)_3$ and N – H bonds indicates higher degree of polymerization and crystallization [38,42]. The ratios followed the order of BCN-T550 (1.02) < BCN-NaK (3.53) < BCN-LiK (5.61) (Table S1). The results were in accordance with the above analysis, that BCN-T550 had amorphous structure, BCN-NaK had amorphous-crystalline isotype heterojunction structure, and BCN-LiK had completely crystalline structure. Fig. 2c and Fig. S4 present that K and Li signals were not detected in the

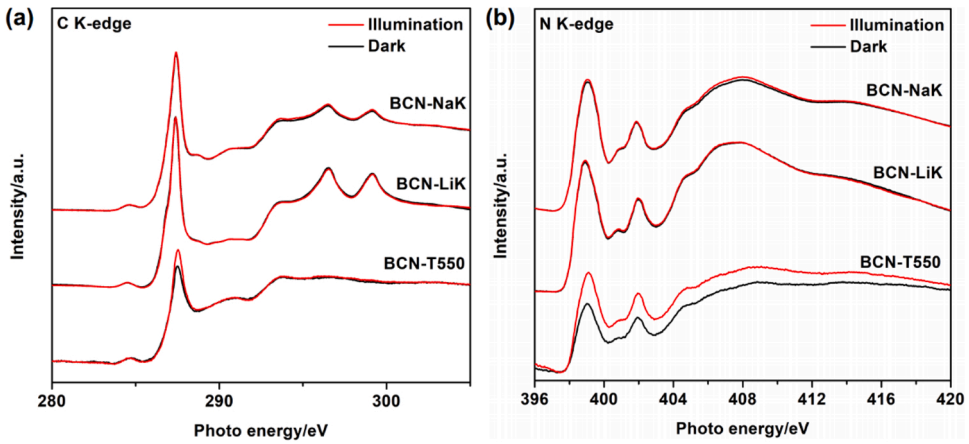

Fig. 5. (a) C and (b) N K-edge XANES spectra for BCN-T550, BCN-LiK and BCN-NaK in dark or with illumination.

XPS spectra of BCN-LiK, while Fig. 2c and Fig. S5 present that there existed K and Na in BCN-NaK structure, the comparison indicated the crystalline BCN-LiK mainly composed of ordered arrangement of heptazine, while BCN-NaK had the components of Na-PHI and K-PHI. Fig. 2d shows that both BCN-LiK and BCN-NaK had little Cl doping in structures.

Synchrotron-based X-ray absorption near-edge structure (XANES) spectroscopy was employed to further elucidate the difference of the three kinds of carbon nitrides for the view of electronic structure evolution. For the C K-edge XANES spectra (Fig. 3a), BCN-T550, BCN-LiK and BCN-NaK showed similar intensities of C1 peaks, demonstrating those carbon nitrides samples possessed carbon defect structures in frameworks. Generally, the intensity of peak C2 can reflect the crystallinity or structural disorder of carbon nitride structure [42]. As compared to BCN-T550, BCN-LiK and BCN-NaK all had much stronger C2 intensities, and BCN-LiK had the highest peak intensity, indicating BCN-LiK possessed high crystallinity and BCN-NaK was partially crystallized, and this result was in accord with the previous results. In addition, BCN-LiK and BCN-NaK showed peaks in the σ * region, and it was also showed that BCN-LiK had stronger peak intensity than BCN-NaK, meaning crystalline structure could result in more photo-excited states with wider spectrum range for carbon nitride [14]. With regard to the N K-edge XANES spectra (Fig. 3b), all the samples showed similar peak distributions, while BCN-NaK and BCN-LiK showed higher intensities than BCN-T550. This phenomenon suggested that more electron excitations from N 1 s to N 2p π * states were generated in crystalline structure than that in amorphous structure for carbon nitride [42,43]. In addition, electron paramagnetic resonance (EPR) spectra are shown to display the concentration of unpaired electrons (Fig. 3c). Note that intensity of EPR is positively correlated with the concentration of unpaired electrons, and nitrogen defects (including nitrogen vacancies and cyano groups) in heptazine units could offer unsaturated sites to facilitate the formation of unpaired electrons [34,38]. Therefore, the contents of nitrogen defects for the samples followed their order of peak intensities, that was demonstrated as BCN-LiK < BCN-T550 < BCN-NaK. According to the previous analysis, the high content of nitrogen defect for BCN-NaK was attributed to the abundant cyano groups. The molecular structure of BCN-NaK was proposed and shown in Fig. 3d and e. BCN-NaK possessed an isotype heterojunction structure constructed by amorphous carbon nitride and crystalline PHI, and plentiful cyano groups were embedded in heptazine rings. Na^+ and K^+ ions were incorporated into void constructed by heptazine-based rings.

3.2. Photocatalytic performance for photocatalysts

Photocatalytic H_2-production reaction was performed to evaluate the performance of the three kind of carbon nitrides. As show in Fig. 4a and Fig. S6, BCN-NaK showed the highest photocatalytic H_2-production rate (26,900 μmol h^{-1} g_{cat}^{-1}), and BCN-LiK ranked second and showed better photocatalytic H_2-production activity (18,220 μmol h^{-1} g_{cat}^{-1}) than BCN-T550 (6512 μmol h^{-1} g_{cat}^{-1}). These results demonstrated that high-cyano groups-content and constructing amorphous-crystalline isotype heterojunction could greatly enhance the photocatalytic H_2-production activity for carbon nitride. Furthermore, when optimizing the photocatalytic system with adding K_2HPO_4 [44], BCN-NaK showed the further enhanced photocatalytic H_2-production activity with the rate reaching 48,656 μmol h^{-1} g_{cat}^{-1}. Therewith the AQYs of BCN-NaK for H_2 production were measured at different wavelengths (Fig. 4b), and an ultrahigh value was achieved to be 68.9 % at 405 nm. Table S2 displays the comparison of BCN-NaK and many representative carbon nitride photocatalysts in the view of photocatalytic H_2 production, BCN-NaK ranked top level. In addition, Fig. 4c presents the cyclic test of photocatalytic H_2 production for BCN-NaK. There was little decay in five cyclic tests (15 h) for photocatalytic H_2 production, thus indicating that BCN-NaK possessed good photocatalytic stability. To demonstrate whether the cyano groups changed during the photocatalytic reaction, FTIR measurement was employed to characterize the recovered photocatalyst (BCN-NaK-R) after photocatalytic H_2-production reaction (Fig. S7). There was little difference between BCN-NaK-R and BCN-NaK in the FTIR spectra. BCN-NaK-R also had much strong peak at 2178 cm^{-1} assigned to the asymmetric stretching vibration of cyano groups (-C≡N), and the peak intensity was similar to that of BCN-NaK. The results indicated the structure of BCN-NaK was unchanged during the photocatalytic H_2 production. Specially, Supplementary Video was taken to intuitively demonstrate the ultrahigh photocatalytic H_2-production activity of BCN-NaK, and it could be seen that innumerable hydrogen gas bubbles quickly generated and broke away from photocatalyst with light irradiation. What's more, the three kinds of carbon nitrides were also applied in photocatalytic CO_2 reduction (Fig. 4d), and the reaction was conducted with no metal cocatalyst and sacrificial agent adding. BCN-NaK still possessed highest photocatalytic CO evolution activity (22.8 μmol h^{-1} g_{cat}^{-1}) as compared to BCN-LiK and BCN-T550, and the selectivity of CO was 61.3 %. The activity was nevertheless better than many reported carbon nitrides on the same photocatalytic condition, indicating the promising efficiency for constructing high-cyano groups-content and amorphous-crystalline isotype heterojunction structure for carbon nitride.

Supplementary material related to this article can be found online at doi:10.1016/j.apcatb.2023.122733.

3.3. Photoexcitation processes and photo-generated charge carriers dynamics for photocatalysts

According to the photocatalytic H_2 production results, difference in carbon nitride structures led to difference in photocatalytic activities. As

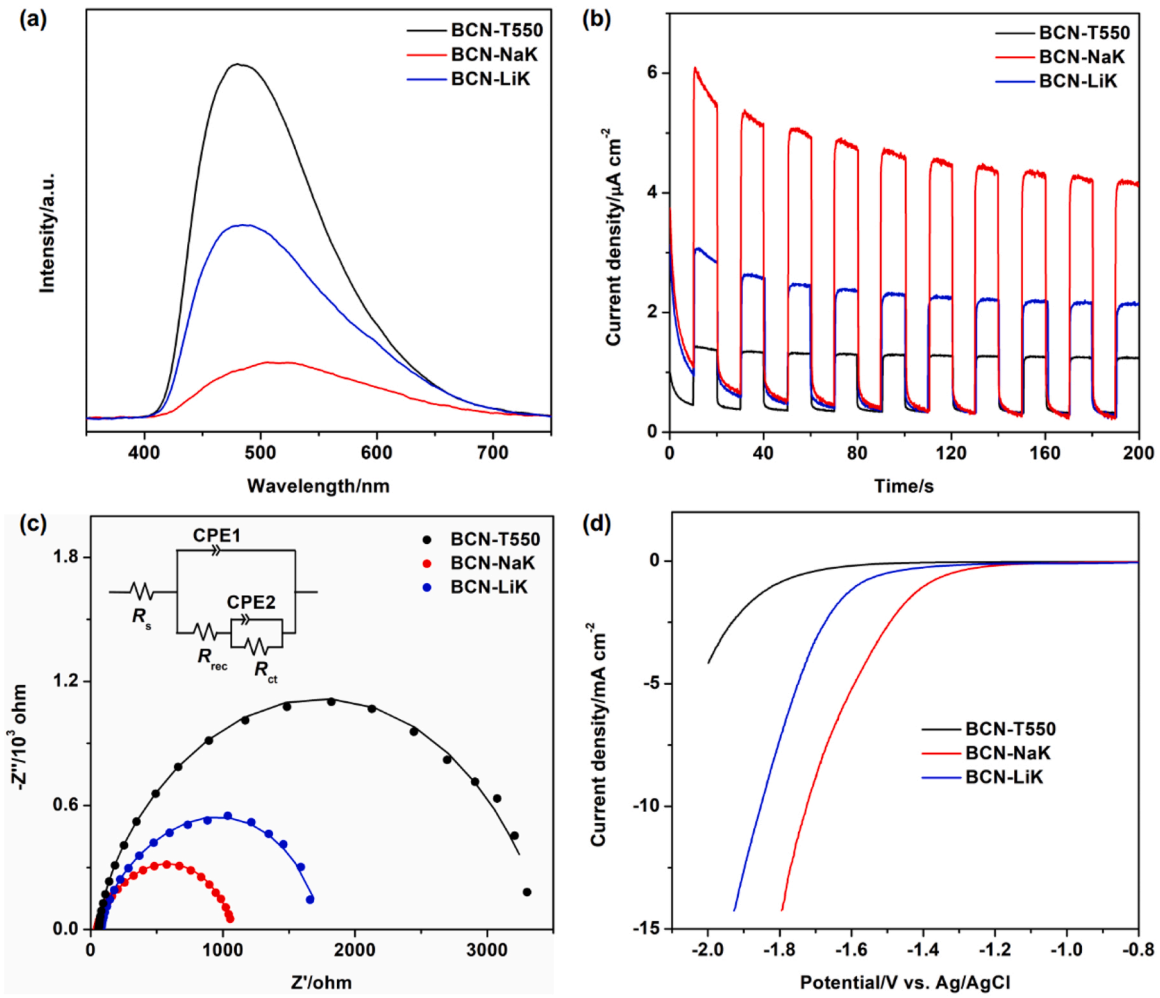

Fig. 6. (a) PL, (b) transient photocurrent density, (c) EIS, and (d) LSV curves for BCN-T550, BCN-LiK and BCN-NaK. The inset in c shows the equivalent circuit. R_s: series resistance, R_{rec}: recombination resistance at the electrode interface, R_{ct}: charge transfer resistance from the electrode to the electrolyte, CPE1 and CPE2: constant phase elements.

many studies have reported, high crystallinity and cyano groups construction can significantly improve the photocatalytic H_2-production activity of carbon nitride. To investigate the predominant role in boosting photocatalytic performance for BCN-LiK and BCN-NaK, light adsorption ability, surface area and photo-generated charge carriers dynamics of these photocatalysts were systematically analyzed. Fig. S8 presents the UV–vis spectraand bandgaps of the photocatalysts. The bandgaps of BCN-T550, BCN-LiK and BCN-NaK were recorded as 2.52, 2.61 and 2.42 eV, respectively. The three kinds of carbon nitrides had similar light absorption ability. With respect to the surface areas of photocatalysts, in general, larger surface area can lead to higher photocatalytic activity. However, BCN-LiK and BCN-NaK had bulk structure and similar surface areas which both were smaller than BCN-T550 (Fig. S9 and Table S3), this paradoxical phenomenon implied that surface area did not play decisive role on determining the enhancement of photocatalytic performance. For exploring the structure benefits for the photoexcitation situation of photocatalyst, the C K-edge and N K-edge XANES spectra for BCN-T550, BCN-LiK and BCN-NaK were conducted under illumination and in the dark. BCN-T550 showed evident irradiation-dark intensity variations for C2 peak in C K-edge spectra and all peaks in N K-edge spectra (Fig. 5a and b), indicating nitrogen defects in amorphous BCN-T550 structure provided plenty of unsaturated sites with unpaired electrons to generate the photo-induced charge carriers [38,42]. However, although BCN-NaK contained lots of cyano groups, the peak intensity variations for BCN-NaK in XANES spectra was extremely small and quite similar to that for BCN-LiK which was not detected to have obvious defects. Both BCN-NaK and BCN-LiK showed little irradiation-dark intensity variation in the whole C K-edge and N K-edge XANES spectra, respectively, thus indicating that cyano groups in BCN-NaK structure did not work for generating photo-induced charge carriers.

As discussed above, high crystallinity and cyano groups construction made limited contribution to light absorption and surface areas, which were both not dominant contribution for elevating photocatalytic performance. Subsequently, the dynamics of pivotal photo-generated charge carries transfer for these photocatalysts were investigated. Firstly, the photoluminescence (PL) spectra were performed to demonstrate the separation and recombination rates of charge carriers (Fig. 6a). In contrast to the strong emission PL peak intensity for BCN-T550, the PL intensity for crystalline BCN-LiK significantly decreased. Furtherly, BCN-NaK showed extremely the weakest PL peak intensity, demonstrating that the recombination of photo-generated electron-hole pairs was effectively suppressed [45,46]. Secondly, (photo)electrochemical measurements were also performed to explore the charge-transfer properties at the catalyst/solution interface. In Fig. 6b, transient photocurrent density curves showed BCN-NaK had highest photocurrent density, followed by BCN-LiK, and BCN-T550 came in last. The result indicated BCN-NaK and BCN-LiK possessed much efficient separation and migration for photo-excited charge carriers under light irradiation as compared to BCN-T550, and especially BCN-NaK behaved

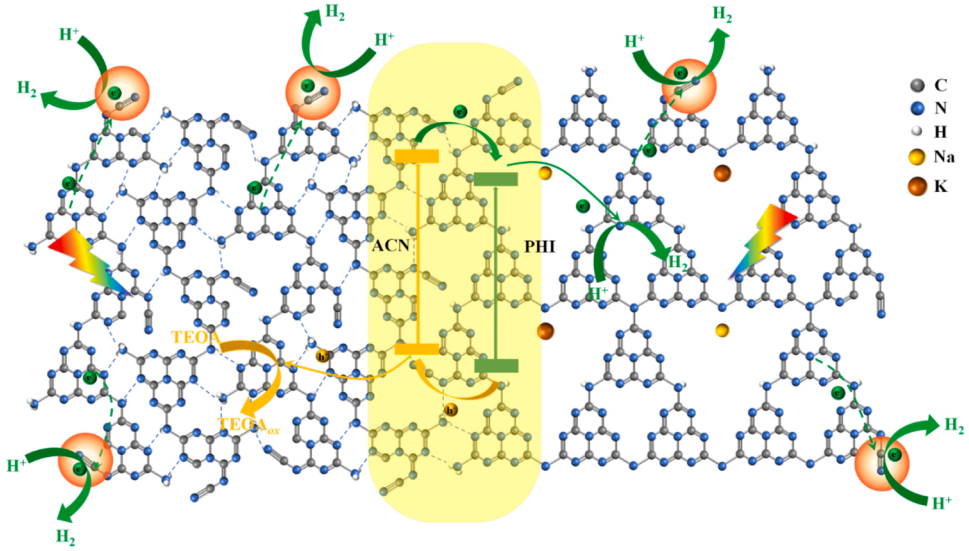

Fig. 7. Schematic mechanism of BCN-NaK for photocatalytic H_2 production.

outstandingly [40]. In addition, electrochemical impedance spectroscopy (EIS) plots showed BCN-NaK had the smallest arc radius, and BCN-LiK had smaller arc radius than BCN-T550 (Fig. 6c), indicating charge-transfer impedance between electrode and electrolyte was followed the order of BCN-NaK < BCN-LiK < BCN-T550. Fig. 6d shows the linear sweep voltammetry (LSV) curves of catalyst for H_2 evolution reaction, it clearly demonstrated BCN-NaK had excellent performance as compared to BCN-LiK and BCN-T550, and BCN-LiK behaved better than BCN-T550. As a result, on one hand, the significantly enhanced charge carries transfer ability for the carbon nitride was the dominant role for boosting the photocatalytic performance. On the other hand, all the above analysis proved that improving the crystallinity of carbon nitride (BCN-NaK and BCN-LiK) could effectively suppress the recombination of photo-generated electron-hole pairs to promote charge carries transfer and thus enhance the photocatalytic H_2 production activity as compared to amorphous carbon nitride (BCN-T550). In addition, cyano groups and amorphous-crystalline isotype heterojunction played crucial role in promoting the separation and migration of photo-generated charge carriers, which made BCN-NaK take the most efficient utilization of charge carriers compared to BCN-T550 and BCN-LiK.

Based on the above analysis, for the photocatalytic H_2 production, the mechanism for the great improvement of H_2 production for BCN-NaK could be proposed and illustrated in Fig. 7. Upon illumination, on one hand, abundant cyano groups, as electron acceptors, could capture photo-excited electrons to promote photo-excited charge carriers effectively separated. One the other hand, BCN-NaK was composed of PHI and cyano groups modified amorphous carbon nitride. Density functional theory (DFT) calculations were carried out to further reveal the bandgap structures of the PHI and cyano groups modified amorphous carbon nitride. The calculated bandgap for cano groups modified amorphous carbon nitride was 2.48 eV, which was very close to the experiment result in view that the bandgap for BCN-T550 based on the Tauc plot was 2.52 eV. The calculated bandgap for PHI was 2.30 eV. The conduction band minimum (CBM) and valence band maximum (VBM) of cyano groups modified amorphous carbon nitride were calculated as − 1.05 and − 3.53 eV vs. vacuum level, respectively. The CBM and VBM of PHI were calculated as − 2.33 and − 4.63 eV vs. vacuum level, respectively (Fig. S11). Thus, an intimate Type II isotype heterojunction was constructed by crystalline PHI and cano groups modified amorphous carbon nitride (ACN) and could effectively promote the separation and migration of photo-excited electrons and holes. As a result, the synergistic promotions made for that the photo-excited electrons were efficiently and maximally involved in water reduction reaction for H_2 production, thus resulting in a breakthrough in photocatalytic H_2 production efficiency.

4. Conclusion

In summary, amorphous carbon nitride (BCN-T550), crystalline carbon nitride (BCN-LiK), and high-cyano groups-content and amorphous-crystalline carbon nitride isotype heterojunction (BCN-NaK) were prepared without eutectic salt, within LiCl/KCl and NaCl/KCl eutectic salts, respectively. BCN-NaK showed higher photocatalytic activities than BCN-LiK and BCN-T550 for both H_2 production and CO_2 reduction. Especially, BCN-NaK achieved an excellent photocatalytic H_2 production efficiency with the AQY of 68.9 % at 405 nm. The enhanced photocatalytic activity of BCN-NaK was mainly attributed to the efficiently facilitated charge transfer ability, which was synergistically promoted by the abundant cyano groups and intimate isotype heterojunction constructed by amorphous carbon nitride and crystalline PHI. This work puts forward a promising strategy for designing novel carbon nitride structure with efficient charge transfer to obtain high photocatalytic performance, and is of significance to promote industrial application.

CRediT authorship contribution statement

Cheng Cheng: Conceptualization, Methodology, Validation, Writing – original draft, Investigation. **Chung-Li Dong, Yu-Cheng Huang** and **Liuhao Mao, Xing Kang** and **Shaohua Shen:** Writing – review & editing. **Jinwen Shi:** Writing – review & editing, Supervision, Project administration, Resources, Funding acquisition. **Liejin Guo**: Supervision, Project administration, Resources, Funding acquisition.

Declaration of Competing Interest

The authors declare that they have no known competing financial interests or personal relationships that could have appeared to influence the work reported in this paper.

Data availability

Data will be made available on request.

Acknowledgements

This work is supported by the Basic Science Center Program for Ordered Energy Conversion of the National Natural Science Foundation of China (No. 51888103), the National Natural Science Foundation of China (Nos. 52206276, 52276213 and 22002126), and the Sichuan Science and Technology Program, and the Fundamental Research Funds for the Central Universities. We thank Linyuan Wen from State Key Laboratory of Multiphase Flow in Power Engineering of Xi'an Jiaotong University for the DFT calculation, and thank Jiamei Liu from Instrumental Analysis Center of Xi'an Jiaotong University for the XPS measurement.

Appendix A. Supporting information

Supplementary data associated with this article can be found in the online version at doi:10.1016/j.apcatb.2023.122733.

References

[1] T. Hisatomi, K. Domen, Reaction systems for solar hydrogen production via water splitting with particulate semiconductor photocatalysts, Nat. Catal. 2 (2019) 387–399.
[2] Y. Li, Z. Ren, M. Gu, Y. Duan, W. Zhang, K. Lv, Synergistic effect of interstitial C doping and oxygen vacancies on the photoreactivity of TiO_2 nanofibers towards CO_2 reduction, Appl. Catal. B Environ. 317 (2022), 121773.
[3] C. Gao, J. Low, R. Long, T. Kong, J. Zhu, Y. Xiong, Heterogeneous single-atom photocatalysts: fundamentals and applications, Chem. Rev. 120 (2020) 12175–12216.
[4] Z. Wang, C. Li, K. Domen, Recent developments in heterogeneous photocatalysts for solar-driven overall water splitting, Chem. Soc. Rev. 48 (2019) 2109–2125.
[5] G. Ling, S. Ng, W. Ong, Tailor-engineered 2D cocatalysts: harnessing electron–hole redox center of 2D g-C_3N_4 photocatalysts toward solar-to-chemical conversion and environmental purification, Adv. Funct. Mater. 32 (2022) 2111875.
[6] L. Mao, B. Lu, J. Shi, Y. Zhang, X. Kang, Y. Chen, H. Jin, L. Guo, Rapid high-temperature hydrothermal post treatment on graphitic carbon nitride for enhanced photocatalytic H_2 evolution, Catal. Today 409 (2023) 94–102.
[7] W. Ong, L. Tan, Y. Ng, S. Yong, S. Chai, Graphitic carbon nitride (g-C_3N_4)-based photocatalysts for artificial photosynthesis and environmental remediation: Are we a step closer to achieving sustainability? Chem. Rev. 116 (2016) 7159–7329.
[8] X. Wang, K. Maeda, A. Thomas, K. Takanabe, G. Xin, J. Carlsson, K. Domen, M. Antonietti, A metal-free polymeric photocatalyst for hydrogen production from water under visible light, Nat. Mater. 8 (2019) 76–80.
[9] G. Zhang, L. Lin, G. Li, Y. Zhang, A. Savateev, S. Zafeiratos, X. Wang, M. Antonietti, Ionothermal synthesis of triazine-heptazine-based copolymers with apparent quantum yields of 60% at 420 nm for solar hydrogen production from "sea water", Angew. Chem. Int. Ed. 57 (2018) 9372–9376.
[10] X. Yu, S. Ng, L. Putri, L. Tan, A. Mohamed, W. Ong, Point-defect engineering: leveraging imperfections in graphitic carbon nitride (g-C_3N_4) photocatalysts toward artificial photosynthesis, Small 17 (2021), e2006851.
[11] C. Cheng, J. Shi, F. Du, S. Zong, X. Guan, Y. Zhang, M. Liu, L. Guo, Simply blending Ni nanoparticles with typical photocatalysts for efficient photocatalytic H_2 production, Catal. Sci. Technol. 9 (2019) 7016–7022.
[12] C. Cheng, L. Mao, J. Shi, F. Xue, S. Zong, B. Zheng, L. Guo, $NiCo_2O_4$ nanosheets as a novel oxygen-evolution-reaction cocatalyst in situ bonded on the g-C_3N_4 photocatalyst for excellent overall water splitting, J. Mater. Chem. A 9 (2021) 12299–12306.
[13] S. An, G. Zhang, K. Li, Z. Huang, X. Wang, Y. Guo, J. Hou, C. Song, X. Guo, Self-supporting 3D carbon nitride with tunable n → π* Electronic transition for enhanced solar hydrogenproduction, Adv. Mater. 33 (2021), e2104361.
[14] G. Zhang, G. Li, T. Heil, S. Zafeiratos, F. Lai, A. Savateev, M. Antonietti, X. Wang, Tailoring the grain boundary chemistry of polymeric carbon nitride for enhanced solar hydrogen production and CO_2 reduction, Angew. Chem. Int. Ed. 58 (2019) 3433–3437.
[15] L. Lin, H. Ou, Y. Zhang, X. Wang, Tri-s-triazine-based crystalline graphitic carbon nitrides for highly efficient hydrogen evolution photocatalysis, ACS Catal. 6 (2016) 3921–3931.
[16] C. Cheng, L. Mao, Z. Huang, J. Shi, B. Zheng, Y. Zhang, L. Guo, Bridging regulation in graphitic carbon nitride for band-structure modulation and directional charge transfer towards efficient H_2 evolution under visible-light irradiation, J. Colloid Interface Sci. 601 (2021) 220–228.
[17] Y. Zhang, Z. Huang, J. Shi, X. Guan, C. Cheng, S. Zong, Y. Huangfu, L. Ma, L. Guo, Maleic hydrazide-based molecule doping in three-dimensional lettuce-like graphite carbon nitride towards highly efficient photocatalytic hydrogen evolution, Appl. Catal. B Environ. 272 (272) (2020), 119009.
[18] J. Zhang, X. Chen, K. Takanabe, K. Maeda, K. Domen, J. Epping, X. Fu, M. Antonietti, X. Wang, Synthesis of a carbon nitride structure for visible-light catalysis by copolymerization, Angew. Chem. Int. Ed. 49 (2010) 441–444.
[19] C. Cheng, J. Shi, L. Mao, C. Dong, Y. Huang, S. Zong, J. Liu, S. Shen, L. Guo, Ultrathin porous graphitic carbon nitride from recrystallized precursor toward significantly enhanced photocatalytic water splitting, J. Colloid Interface Sci. 637 (2023) 271–282.
[20] C. Xiao, L. Zhang, H. Hao, W. Wang, High selective oxidation of benzyl alcohol to benzylaldehyde and benzoic acid with surface oxygen vacancies on $W_{18}O_{49}$/holey ultrathin g-C_3N_4 Nanosheets, ACS Sustain. Chem. Eng. 7 (2019) 7268–7276.
[21] Y. Zhang, Z. Chen, J. Li, Z. Lu, X. Wang, Self-assembled synthesis of oxygen-doped g-C_3N_4 nanotubes in enhancement of visible-light photocatalytic hydrogen, J. Energy Chem. 54 (2021) 36–44.
[22] D. Zhu, Q. Zhou, Nitrogen doped g-C_3N_4 with the extremely narrow band gap for excellent photocatalytic activities under visible light, Appl. Catal. B Environ. 281 (2021), 119474.
[23] X. Li, J. Hu, T. Yang, X. Yang, J. Qu, C. Li, Efficient photocatalytic H_2-evolution coupled with valuable furfural-production on exquisite 2D/2D $LaVO_4$/g-C_3N_4 heterostructure, Nano Energy 92 (2022), 106714.
[24] C. Yang, Q. Tan, Q. Li, J. Zhou, J. Fan, B. Li, J. Sun, K. Lv, 2D/2D Ti_3C_2 MXene/g-C_3N_4 nanosheets heterojunction for high efficient CO_2 reduction photocatalyst: dual effects of urea, Appl. Catal. B Environ. 268 (2020), 118738.
[25] L. Lin, Z. Yu, X. Wang, Crystalline carbon nitride semiconductors for photocatalytic water splitting, Angew. Chem. Int. Ed. 58 (2019) 6164–6175.
[26] M. Liu, C. Wei, H. Zhuzhang, J. Zhou, Z. Pan, W. Lin, Z. Yu, G. Zhang, X. Wang, Fully condensed poly(triazine imide) crystals: extended π-conjugation and structural defects for overall water splitting, Angew. Chem. Int. Ed. 61 (2022), e202113389.
[27] L. Lin, Z. Lin, J. Zhang, X. Cai, W. Lin, Z. Yu, X. Wang, Molecular-level insights on the reactive facet of carbon nitride single crystals photocatalysing overall water splitting, Nat. Catal. 3 (2020) 649–655.
[28] K. Li, W. Zhou, X. Li, Qin Li, S. Carabineiro, S. Zhang, J. Fan, K. LV, Synergistic effect of cyano defects and $CaCO_3$ in graphitic carbon nitride nanosheets for efficient visible-light-driven photocatalytic NO removal, J. Hazard. Mater. 442 (2023), 130040.
[29] Y. Zhao, P. Zhang, Z. Yang, L. Li, J. Gao, S. Chen, T. Xie, C. Diao, S. Xi, B. Xiao, C. Hu, W. Choi, Mechanistic analysis of multiple processes controlling solar-driven H_2O_2 synthesis using engineered polymeric carbon nitride, Nat. Commun. 12 (2021) 3701.
[30] G. Liu, G. Zhao, W. Zhou, Y. Liu, H. Pang, H. Zhang, D. Hao, X. Meng, P. Li, T. Kako, J. Ye, In situ bond modulation of graphitic carbon nitride to construct p-n homojunctions for enhanced photocatalytic hydrogen production, Adv. Funct. Mater. 26 (2016) 6822–6829.
[31] F. Dong, Z. Zhao, T. Xiong, Z. Ni, W. Zhang, Y. Sun, W.K. Ho, In situ construction of g-C3N4/g-C3N4 metal-free heterojunction for enhanced visible-light photocatalysis, ACS Appl. Mater. Interfaces 5 (2013) 11392–11401.
[32] D. Zhao, Y. Wang, C.-L. Dong, Y.-C. Huang, J. Chen, F. Xue, S. Shen, L. Guo, Boron-doped nitrogen-deficient carbon nitride-based Z-scheme heterostructures for photocatalytic overall water splitting, Nat. Energy 6 (2021) 388–397.
[33] S. Shen, J. Chen, Y. Wang, C.-L. Dong, F. Meng, Q. Zhang, Y. Huangfu, Z. Lin, Y.-C. Huang, Y. Li, M. Li, L. Gu, Boosting photocatalytic hydrogen production by creating isotype heterojunctions and single-atom active sites in highly-crystallized carbon nitride, Sci. Bull. 67 (2022) 520–528.
[34] C. Cheng, J. Shi, L. Wen, C.-L. Dong, Y.-C. Huang, Y. Zhang, S. Zong, Z. Diao, S. Shen, L. Guo, Disordered nitrogen-defect-rich porous carbon nitride photocatalyst for highly efficient H_2 evolution under visible-light irradiation, Carbon 181 (2021) 193–203.
[35] G. Zhang, M. Liu, T. Heil, S. Zafeiratos, A. Savateev, M. Antonietti, X. Wang, Electron deficient monomers that optimize nucleation and enhance the photocatalytic redox activity of carbon nitrides, Angew. Chem. Int. Ed. 58 (2019) 14950–14954.
[36] Y. Li, D. Zhang, J. Fan, Q. Xiang, Highly crystalline carbon nitride hollow spheres with enhanced photocatalytic performance, Chin. J. Catal. 42 (2021) 627–636.
[37] T. Miller, T.M. Suter, A. Telford, L. Picco, O. Payton, F. Russell-Pavier, P. Cullen, A. Sella, M. Shaffer, J. Nelson, V. Tileli, P. McMillan, C. Howard, Single crystal, luminescent carbon nitride nanosheets formed by spontaneous dissolution, Nano Lett. 17 (2017) 5891–5896.
[38] C. Cheng, C.-L. Dong, J. Shi, L. Mao, Y.-C. Huang, X. Kang, S. Zong, S. Shen, Regulation on polymerization degree and surface feature in graphitic carbon nitride towards efficient photocatalytic H_2 evolution under visible-light irradiation, J. Mater. Sci. Technol. 98 (2022) 160–168.
[39] J. Kroger, F. Podjaski, G. Savasci, I. Moudrakovski, A. Jimenez-Solano, M. Terban, S. Bette, V. Duppel, M. Joos, A. Senocrate, R. Dinnebier, C. Ochsenfeld, B. Lotsch, Conductivity mechanism in ionic 2D carbon nitrides: from hydrated ion motion to enhanced photocatalysis, Adv. Mater. 34 (2022), e2107061.
[40] C. Cheng, S. Zong, J. Shi, F. Xue, Y. Zhang, X. Guan, B. Zheng, J. Deng, L. Guo, Facile preparation of nanosized MoP as cocatalyst coupled with g-C_3N_4 by surface bonding state for enhanced photocatalytic hydrogen production, Appl. Catal. B Environ. 265 (2020), 118620.
[41] Y. Zhang, J. Shi, Z. Huang, X. Guan, S. Zong, C. Cheng, B. Zheng, L. Guo, Synchronous construction of CoS_2 in-situ loading and S doping for g-C_3N_4: enhanced photocatalytic H_2-evolution activity and mechanism insight, Chem. Eng. J. 401 (2020), 126135.
[42] D. Zhao, C.L. Dong, B. Wang, C. Chen, Y.C. Huang, Z. Diao, S. Li, L. Guo, S. Shen, Synergy of dopants and defects in graphitic carbon nitride with exceptionally modulated band structures for efficient photocatalytic oxygen evolution, Adv. Mater. 31 (2019), e1903545.
[43] D. Zhao, J. Chen, C.-L. Dong, W. Zhou, Y.-C. Huang, S.S. Mao, L. Guo, S. Shen, Interlayer interaction in ultrathin nanosheets of graphitic carbon nitride for efficient photocatalytic hydrogen evolution, J. Catal. 352 (2017) 491–497.

[44] G. Liu, T. Wang, H. Zhang, X. Meng, D. Hao, K. Chang, P. Li, T. Kako, J. Ye, Nature-inspired environmental "phosphorylation" boosts photocatalytic H_2 production over carbon nitride nanosheets under visible-lighirradiation, Angew. Chem. Int. Ed. 54 (2015) 13561–13565.

[45] W. Dai, J. Long, L. Yang, S. Zhang, Y. Xu, X. Luo, J. Zou, S. Luo, Oxygen migration triggering molybdenum exposure in oxygen vacancy-rich ultra-thin Bi_2MoO_6 nanoflakes: Dual binding sites governing selective CO_2 reduction into liquid hydrocarbons, J. Energy Chem. 61 (2021) 281–289.

[46] W. Dai, J. Yu, S. Luo, X. Hu, L. Yang, S. Zhang, B. Li, X. Luo, J. Zou, WS_2 quantum dots seeding in Bi_2S_3 nanotubes: a novel Vis-NIR light sensitive photocatalyst with low-resistance junction interface for CO_2 reduction, Chem. Eng.. J. 389 (2020), 123430.